Aluminum abundance on the surface of Mercury: Application of a new background-reduction technique for the analysis of gamma-ray spectroscopy data

Patrick N. Peplowski,[1] Edgar A. Rhodes,[1] David K. Hamara,[2] David J. Lawrence,[1] Larry G. Evans,[3] Larry R. Nittler,[4] and Sean C. Solomon[4,5]

Received 2 July 2012; revised 24 September 2012; accepted 7 October 2012; published 7 December 2012.

[1] A new technique has been developed for characterizing gamma-ray emission from a planetary surface in the presence of large background signals generated in a spacecraft. This technique is applied to the analysis of Al gamma rays measured by the MESSENGER Gamma-Ray Spectrometer to determine the abundance of Al on the surface of Mercury. The result (Al/Si = $0.29^{+0.05}_{-0.13}$) is consistent with Al/Si ratios derived from the MESSENGER X-Ray Spectrometer and confirms the finding of low Al abundances. The measured abundance rules out a global, lunar-like feldspar-rich crust and is consistent with previously suggested analogs for surface material on Mercury, including terrestrial komatiites, low-iron basalts, partial melts of CB chondrites, and partial melts of enstatite chondrites. Additional applications of this technique include the measurement of other elements on Mercury's surface as well as the analysis of data from other planetary gamma-ray spectrometer experiments.

Citation: Peplowski, P. N., E. A. Rhodes, D. K. Hamara, D. J. Lawrence, L. G. Evans, L. R. Nittler, and S. C. Solomon (2012), Aluminum abundance on the surface of Mercury: Application of a new background-reduction technique for the analysis of gamma-ray spectroscopy data, *J. Geophys. Res.*, *117*, E00L10, doi:10.1029/2012JE004181.

1. Introduction

[2] Gamma-ray spectroscopy is a well-established technique for the remote characterization of the elemental composition of planetary surfaces, as has been demonstrated by its successful utilization from orbit around the Moon [e.g., *Bielefeld et al.*, 1976; *Lawrence et al.*, 1998; *Yamashita et al.*, 2010] and Mars [*Boynton et al.*, 2007] and by the MErcury Surface, Space ENviroment, GEochemisty, and Ranging (MESSENGER) spacecraft at Mercury [*Peplowski et al.*, 2011b; *Evans et al.*, 2012]. The Dawn spacecraft is also carrying a gamma-ray spectrometer to characterize the surface compositions of asteroids 4 Vesta and 1 Ceres [*Prettyman et al.*, 2011]. The development of new data analysis algorithms can improve the capability of gamma-ray spectrometer data sets to address the near-surface elemental compositions of these bodies. This work presents a novel technique for reducing a measured gamma-ray signal into its spacecraft- and planet-originating components, facilitating the isolation of the planetary signal of interest in the presence of backgrounds with comparable intensity.

[3] Gamma-ray spectroscopy of non-radioactive elements relies on the excitation of atomic nuclei by neutrons originating from surface-incident galactic cosmic ray (GCR) proton-induced spallation reactions [e.g., *Reedy*, 1978]. The excited nuclei decay to stable states by emitting gamma rays at element-characteristic energies, facilitating the characterization of the elemental composition of the surface from orbit. A major difficulty of gamma-ray spectroscopy is the need to characterize elemental abundances in the presence of large, spacecraft-generated backgrounds. These backgrounds exist for elements in materials that are present within the spacecraft, particularly those closest to the detector. These elements often include Al, Fe, Ti, and Mg, which are major elements in surface rocks, and their abundances are therefore frequently of geochemical interest. Since these backgrounds originate from the same processes that produce the planet-originating signal, they are spectroscopically indistinguishable.

[4] Lunar Prospector [*Feldman et al.*, 2004] and Mars Odyssey [*Boynton et al.*, 2004] utilized boom-mounted gamma-ray spectrometers (GRSs) to reduce the detection of spacecraft-originating background gamma rays. However, in the case of the Mars Odyssey GRS this precaution did not eliminate all spacecraft backgrounds [*Evans et al.*, 2006] because of the relatively large amount of material in the immediate vicinity of the sensor (e.g., Ti) and to the fact that GRS-measured backgrounds are dominated by the material

[1]The Johns Hopkins University Applied Physics Laboratory, Laurel, Maryland, USA.
[2]Lunar and Planetary Laboratory, University of Arizona, Tucson, Arizona, USA.
[3]Computer Sciences Corporation, Lanham-Seabrook, Maryland, USA.
[4]Department of Terrestrial Magnetism, Carnegie Institution of Washington, Washington, D. C., USA.
[5]Lamont-Doherty Earth Observatory, Columbia University, Palisades, New York, USA.

Corresponding author: P. N. Peplowski, The Johns Hopkins University Applied Physics Laboratory, 11100 Johns Hopkins Rd., Laurel, MD 20723, USA. (patrick.peplowski@jhuapl.edu)

0148-0227/12/2012JE004181

closest to the sensor. Body-mounted GRS instruments, such as those on the Near Earth Asteroid Rendezvous (NEAR) [*Goldsten et al.*, 1997], SELenological and ENgineering Explorer (SELENE) [*Hasebe et al.*, 2008], MESSENGER [*Goldsten et al.*, 2007], and Dawn spacecraft, are subject to much larger backgrounds, and in the case of the NEAR GRS this issue contributed to the inability of the instrument to make compositional measurements of the surface of 433 Eros from orbit [*Trombka et al.*, 2001]. Analysis of MESSENGER GRS measurements made during the three Mercury flybys highlighted the substantial contribution of spacecraft-originating backgrounds to the measured signal, as well as the difficulties associated with determining the elemental composition of Mercury in their presence [*Rhodes et al.*, 2011].

[5] The technique presented here for determining the abundances of elements on a planetary surface in the presence of large, spacecraft-originating gamma-ray backgrounds requires the identification of two gamma-ray photopeaks from the element of interest, along with knowledge of the relevant gamma-ray production cross sections, the energy-dependent flux of the source neutrons, and the altitude-dependence of their measured count rates. The usefulness of this technique is demonstrated by presenting it in the context of a measurement of Al on the surface of Mercury. This measurement would normally be impossible because of the unknown magnitude of the Al background, which results from neutron-induced reactions within Al immediately surrounding the sensor. The validity of this result has been confirmed through a comparison with complementary measurements of Mercury's surface composition by the MESSENGER X-Ray Spectrometer (XRS) [*Nittler et al.*, 2011; *Weider et al.*, 2012], for which the Al signal represents a collimated view of the planet and therefore does not include spacecraft backgrounds. A discussion of the utilization of this technique to additional elements on the surface of Mercury as well as to other ongoing and future gamma-ray spectroscopy data sets is also presented.

2. MESSENGER Gamma-Ray Spectrometer Al Measurements

[6] The MESSENGER GRS measures detector-incident gamma rays throughout the spacecraft's highly eccentric orbit about Mercury, which ranged in altitude from 200 to 15,200 km above the surface during the primary mission [*Solomon et al.*, 2007]. The varying altitude and attitude of the spacecraft relative to Mercury, coupled with the altitude-dependence of the gamma-ray flux, complicates the analysis of MESSENGER GRS data [*Peplowski et al.*, 2011a, 2012]. Fortunately, this altitude dependence also provides a mechanism for separating the measured gamma-ray signal into its individual constituents, facilitating the characterization of the planet-originating signal of interest.

[7] This study uses the gamma rays from Al at 1014 and 2211 keV energy that result from neutron inelastic scattering reactions in the near surface of Mercury and within the spacecraft. The increase in the measured count rates for these gamma rays close to Mercury is demonstrated in Figure 1, which compares high- and low-altitude measurements of these spectral regions. Following the methodology of *Peplowski et al.* [2011b], high- and low-altitudes are defined to be >14,000 km and <2,000 km respectively. The presence of Al gamma rays in the high-altitude spectrum, which was acquired too far from the planet to have a resolvable contribution from the surface, indicates the existence of a non-planetary Al background contribution to the GRS-measured gamma-ray spectrum. That these Al gamma rays were also observed during the 6.6-year interplanetary journey en route to Mercury orbit insertion [*Goldsten et al.*, 2007] conclusively demonstrates that there is a non-planetary component to the observed peaks. The measured count rates for these gamma rays were determined by fitting the regions of interest with exponentially modified Gaussian functions and a polynomial background to determine the peak areas, following the procedure detailed by *Peplowski et al.* [2011b].

[8] Prior to characterizing the nature of the altitude dependence of the Al gamma-ray signals, it is necessary to remove variations in these count rates due to other effects, of which two have been identified: time-dependent changes in the signal-inducing GCR flux and spacecraft off-nadir pointing. Variations in the GCR flux can lead to time-dependent gamma-ray emission from the planetary surface and the spacecraft. To avoid this complication, the analysis here is limited to data acquired during the first 59 days of orbital science operations, a time period that experienced little variation in the GCR flux relative to the statistical uncertainties of the gamma-ray measurements [*Peplowski et al.*, 2012]. The GCR flux was characterized with the MESSENGER Neutron Spectrometer (NS) triple-coincidence counter following the methodology of *Feldman et al.* [2010]. This interval was also chosen because it represents one sidereal day on Mercury, which coupled with the nature of the MESSENGER orbit about Mercury ensures that this analysis includes even coverage of all longitudes on the surface. Due to MESSENGER's highly eccentric orbit about Mercury, the GRS coverage of the surface is biased in latitude toward regions nearest periapsis (55–65°N for the period treated here).

[9] The second source of non-planetary variation in the measured Al gamma-ray count rates is off-nadir instrument pointing. Off-nadir pointing reduces the sensitivity of the GRS to the planet-originating signal as the result of the attenuation of gamma rays by GRS-surrounding spacecraft components. Low-altitude data used in this analysis are limited to those collected at nadir angles <45°, because gamma-ray attenuation is not significant for these angles for the 1779-keV Si peak [*Peplowski et al.*, 2012], which is known to be dominated by planet-originating gamma rays [*Evans et al.*, 2012]. The removal of off-nadir pointing data reinforces the bias of these measurements to northern regions, as it disproportionately removes data south of the periapsis latitude (see Figure 2).

[10] The selection of data that are not influenced by the time-dependence of the GCR flux and the off-nadir viewing geometries facilitates a characterization of the Al gamma rays (γ) as a function of altitude (Figure 3). This characterization is accomplished by summing GRS spectra by the altitude of the spacecraft and determining the Al peak areas for each summed spectrum. These peak areas are corrected for the total data acquisition time and the detector live time to determine the altitude-dependent count rate (C_γ^m) at the detector (Figure 3). Determining the abundance of Al on the surface of Mercury requires determining the fraction of C_γ^m

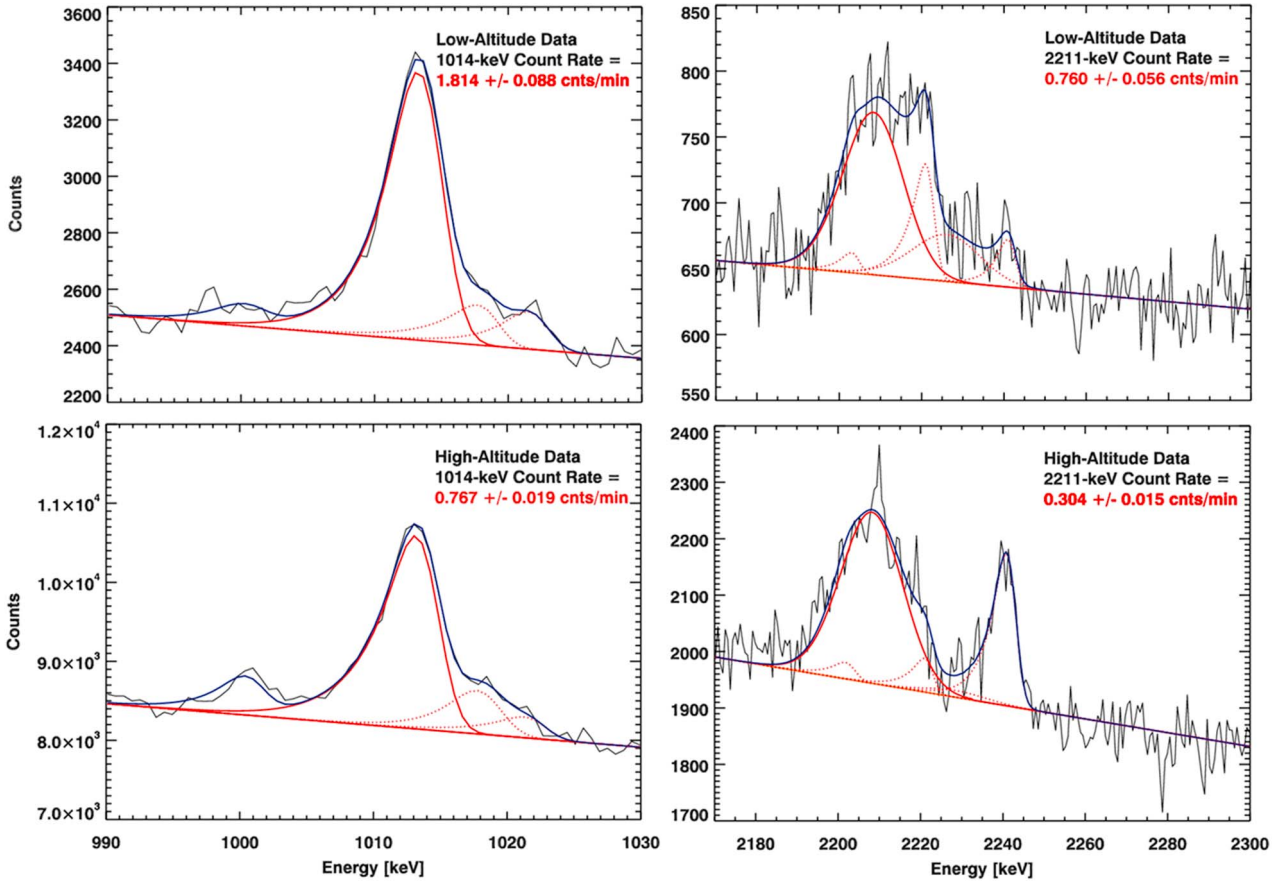

Figure 1. Summed gamma-ray spectra (black) in the region of the 1014- and 2211-keV gamma rays at high- (>14,000 km) and low- (<2,000 km) altitudes. Fits to the 1014- and 2211-keV peaks and the background continuum are shown in solid red, overlapping peaks are shown as dashed red lines, and the fit to the full spectrum is shown in blue. The fits were carried out following the formalism presented by *Peplowski et al.* [2011b]. Measured count rates are listed on each plot. These data suggest that the measured Al count rates increase with decreasing altitude, but there is clearly a strong high-altitude background signal as well.

that originates from the planet. This task involves segregating the measured signal into its individual components in order to isolate the planet-originating signal of interest from all sources of background.

3. Source Component Analysis

[11] The correlation between the altitude of the MESSENGER spacecraft and the measured Al gamma-ray count rates (Figure 3) indicates the need for an altitude-dependent model for the total gamma-ray flux at the detector. This section details a generic model for characterizing the measured gamma-ray flux as a function of altitude. This model was applied to the MESSENGER GRS-measured Al peaks (as described in section 4) as an example of its use.

[12] The measured gamma-ray flux at the detector (Φ_γ^{m}) can be described in terms of its individual source components, as it originates from three distinct sources: gamma rays arising from spacecraft-incident GCRs ($\Phi_\gamma^{\mathrm{GCR}}$), gamma rays arising from spacecraft-incident neutrons emanating from the planetary surface (Φ_γ^{n}), and gamma rays emanating directly from the planetary surface (Φ_γ^{p}). Φ_γ^{p} is the signal of interest, and $\Phi_\gamma^{\mathrm{GCR}}$ and Φ_γ^{n} are background signals. The relationship between the measured flux and these source components as a function of altitude is

$$\Phi_\gamma^{m}[\Omega(h),t] = \Phi_\gamma^{\mathrm{GCR}}(t)[1-\Omega(h)] + \left[\Phi_\gamma^{\mathrm{n}}(t) + \Phi_\gamma^{p}(t)\right]\Omega(h) \quad (1)$$

where h is the spacecraft altitude and $\Omega(h)$ is the fraction of the unit sphere around the GRS that is subtended by the field of view of the planet (hereafter referred to as the solid angle). Equation (1) is based on the assumption that planet-originating neutrons and gamma rays have identical, isotropic emission from the planet, a choice that is justified in Appendix A. The altitude-dependent solid angle subtended by the planet is

$$\Omega(h) = \frac{\int_0^{2\pi}\int_0^{\theta_{\mathrm{L}}} \sin\theta \mathrm{d}\theta\mathrm{d}\varphi}{\int_0^{2\pi}\int_0^{\pi} \sin\theta \mathrm{d}\theta\mathrm{d}\varphi} = \frac{[1-\cos\theta_{\mathrm{L}}(h)]}{2} \quad (2)$$

where θ_L defines the angle between the spacecraft nadir direction and the horizon as viewed by the GRS:

$$\theta_L(h) = \text{acos}\left[\frac{\sqrt{[R_m + h]^2 - R_M{}^2}}{R_M + h}\right] \quad (3)$$

and R_M is the radius of Mercury (2440 km). As denoted in equation (1), each component (Φ_γ) has a time dependence that is driven by variations in the galactic cosmic ray flux. This time dependence can be removed by correcting the measured gamma-ray flux for variations in the GCR flux over time prior to applying this formalism. For the subset of MESSENGER GRS measurements of Al shown in Figure 3, the time dependence was ignored by utilizing a subset of data over which the GCR flux did not vary appreciably (see section 2). The resulting model for the measured gamma-ray flux in terms of its source components was reduced to a function of spacecraft altitude only.

3.1. Galactic Cosmic Ray-Induced Background

[13] The background component that dominates the GRS measurements far from the planet results from interactions between GCR-induced spallation neutrons generated within the spacecraft itself and the materials that comprise the spacecraft. The spacecraft neutron flux is composed predominantly of fast (>1 MeV) neutrons, so neutron inelastic scattering reactions are the primary source of background. Following typical nuclear reaction conventions for the production of gamma rays by a particle beam incident on a target, the measured gamma-ray flux resulting from this process (Φ_γ^{GCR}) is calculated as

$$\Phi_\gamma^{GCR} = \varepsilon_\gamma N_m \int_{E\,min}^{\infty} \sigma_\gamma(E_n) N_n^{GCR}(E_n) dE \quad (4)$$

where E_{min} is the threshold energy of the neutron inelastic scattering reaction, ε_γ is the energy-dependent gamma-ray detection efficiency, $\sigma_\gamma(E_n)$ is the neutron-energy-dependent gamma-ray production cross section in millibarns (mb; 1 millibarn = 10^{-27} cm^2), N_n^{GCR} is the GCR-induced neutron flux in the spacecraft in neutrons cm^{-2} min^{-1}, and N_m is the effective amount of the material of interest (m) in the spacecraft expressed as the number of atoms seen by the GRS, a quantity that includes the relative attenuation of gamma rays produced by this material and the distance from the GRS. As GCRs illuminate the spacecraft from all directions, and neutrons are produced throughout the structure by highly penetrating GCR protons, we treat N_n^{GCR} as a constant throughout the spacecraft.

3.2. Planet-Originating Signal and Background

[14] Close to the planet, there are two additional sources of gamma rays. The first is the flux emanating from the planetary surface (Φ_γ^p), which is the signal of interest and can be determined only by removing contributions to the measured signal from all other sources. The second source is gamma rays resulting from the excitation of spacecraft materials by neutrons emanating from the planetary surface (Φ_γ^n). Following the formalism presented in equation (4), Φ_γ^n is calculated as

$$\Phi_\gamma^n = \varepsilon_\gamma N_m \int_{E\,min}^{\infty} \sigma_\gamma(E_\gamma) N_n^p(E_n) dE \quad (5)$$

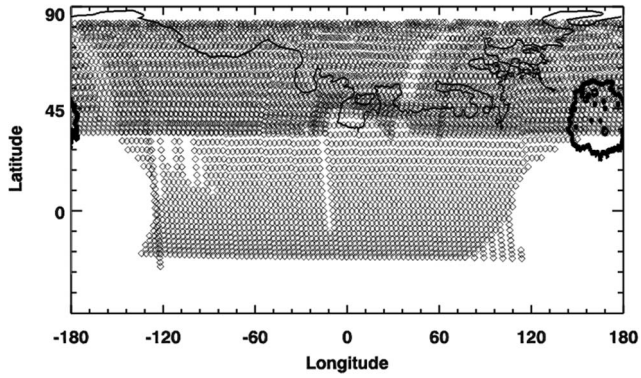

Figure 2. Sub-spacecraft position as a function of latitude and longitude for the data set used in this analysis. The data set is biased toward higher latitudes (>40°N) where the measurement altitudes are lower and coverage of the surface is more complete. The gaps at ±180° longitudes are the result of the restriction to nadir angle ≤45° (see section 2). As a result, the most comparable XRS measurements are the spatially resolved northern plains values of *Weider et al.* [2012]. The location of the northern volcanic plains [*Head et al.*, 2011] is outlined by the thin black line, and the Caloris basin interior plains are outlined by the thick black line. The nature of the MESSENGER orbit and its impact on the coverage of Mercury's surface is discussed in detail by *Peplowski et al.* [2012].

where $N_n^p(E_n)$ is the spacecraft-incident, planet-originating neutron flux resulting from GCRs interacting at the planetary surface. The quantity $N_n^p(E_n)$ is moderated within the spacecraft and is therefore not constant at all points within MESSENGER. However, the GRS is most sensitive to gamma rays produced close to the detector, where gamma-ray attenuation by GRS-surrounding materials is minimal and the probability for detection is larger. This situation is accommodated by the N_m term, which represents the attenuation and distance-weighted amount of material m within the spacecraft. The quantity N_m effectively places less weight on material deep within the spacecraft structure, which is the material that is most affected by the attenuation of the planetary neutrons. As a result, variations of $N_n^p(E_n)$ within the spacecraft structure are assumed to have a negligible effect on the measured Φ_γ^n.

4. Data Reduction

[15] The formalism presented in section 3 can be applied to the analysis of gamma rays from any element. This section will utilize the 1014- and 2211-keV Al gamma rays in the MESSENGER GRS data set (Figure 1) as an example of the application of this technique. This analysis requires converting C_γ^m (Figure 3) to the measured gamma-ray flux at the detector (Φ_γ^m), which was achieved by dividing C_γ^m by the detector area as viewed by the planet for each altitude bin (see Appendix B) and the energy-dependent gamma-ray detection efficiency (ε_γ). The efficiency values ($\varepsilon_{1014} = 0.115 \pm 0.028$ and $\varepsilon_{2211} = 0.060 \pm 0.011$) were derived from radiation transport models of the efficiency of the GRS as described by *Peplowski et al.* [2012], and their errors include the standard deviation of the average value over the illuminated region of the detector and the statistical precision of the simulations.

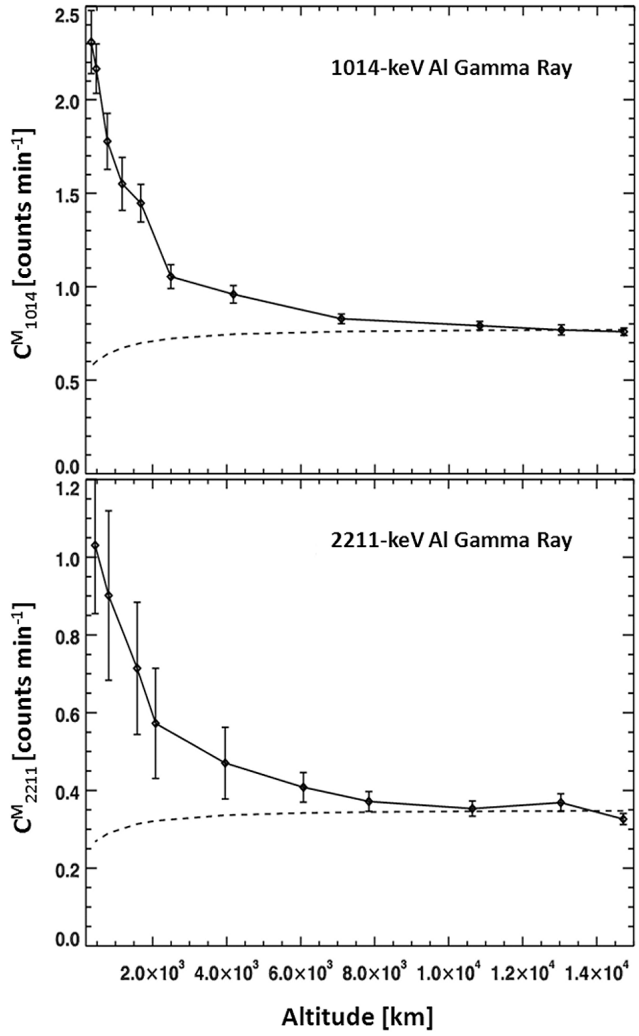

Figure 3. The (top) 1014- and (bottom) 2211-keV gamma-ray count rates (C^M) versus altitude, illustrating the strong altitude dependence of the GRS-measured signal. The dashed line represents the solid-angle-corrected high-altitude count rate, which is the only background component that is separable on the basis of altitude (see section 4).

[16] The first step in applying the source component analysis technique was to remove the Φ_γ^{GCR} component from the measured gamma-ray flux Φ_γ^m. Although equation (4) details a method for calculating Φ_γ^{GCR} directly, the altitude dependence of the signal detailed in equation (1) facilitates a method for removing this background component using the GRS-measured high-altitude count rate only. This method is possible because Φ_γ^{GCR} is directly proportional to the spacecraft-incident GCR flux, which in the regime of time-invariant GCR flux is a function only of the solid angle of the planet. At high altitudes, the solid angle approaches zero and the measured gamma-ray flux (equation (1)) consists entirely of contributions resulting from spacecraft-incident GCRs as

$$\lim_{h\rightarrow\geq 14{,}000\,\mathrm{km}} \Phi_\gamma^m(h) \rightarrow \Phi_\gamma^{GCR}[1-\Omega(h)] \qquad (6)$$

The solid angle does not vary markedly in the high-altitude regime, so equation (6) can be further reduced to

$$\Phi_{1014}^{GCR}(\Omega\rightarrow 0) = \Phi_{1014}^0 = 0.264 \pm 0.080\,\mathrm{counts\,min^{-1}cm^{-2}}$$

$$\Phi_{2211}^{GCR}(\Omega\rightarrow 0) = \Phi_{2211}^0 = 0.200 \pm 0.052\,\mathrm{counts\,min^{-1}cm^{-2}}$$

where Φ_γ^0 was determined from spectral analysis of high-altitude data shown in Figure 1. Quantifying Φ_γ^0 facilitates the reduction of equation (1) to

$$\Phi_\gamma^m(\Omega(h)) = \Phi_\gamma^0[1-\Omega(h)] + \left[\Phi_\gamma^n + \Phi_\gamma^p\right]\Omega(h) \qquad (7)$$

which in turn allows for the definition of a modified measured flux ($\Phi_\gamma^{m'}$) in which the contributions from Φ_γ^{GCR} have been removed:

$$\Phi_\gamma^{m'}(\Omega(h)) = \Phi_\gamma^m(\Omega(h)) - \Phi_\gamma^0[1-\Omega(h)] = \left[\Phi_\gamma^n + \Phi_\gamma^p\right]\Omega(h) \quad (8)$$

This step leaves the planetary-neutron-induced background Φ_γ^n and the signal of interest Φ_γ^p as the remaining contributions to the measured flux (Figure 4).

[17] The quantities Φ_γ^n and Φ_γ^p have identical solid-angle dependencies (Appendix A) and therefore cannot be isolated using the altitude of the spacecraft as was done to remove contributions from Φ_γ^{GCR}. In the case of the 1014- and 2211-keV gamma rays, the model for the measured flux is given by substituting equation (5) into equation (8) to yield

$$\Phi_{1014}^{m'}(\Omega) = \left[N_{Al}\int_{E\mathrm{min}}^{\infty}\sigma_{1014}(E_n)N_n^p(E_n)dE + \Phi_{1014}^p\right]\Omega \qquad (9)$$

$$\Phi_{2211}^{m'}(\Omega) = \left[N_{Al}\int_{E\mathrm{min}}^{\infty}\sigma_{2211}(E_n)N_n^p(E_n)dE + \Phi_{2211}^p\right]\Omega \qquad (10)$$

The energy-dependent gamma-ray production cross sections $\sigma_\gamma(E_n)$ were obtained from evaluated nuclear reaction measurements [*Kim et al.*, 2007] and are shown in Figure 5. The planet-originating, spacecraft-incident neutron flux $N_n^p(E_n)$ is shown in Figure 6 and was calculated with MCNPX radiation transport modeling codes of GCR-induced neutron production (see Appendix C). In principle, the effective amount of spacecraft Al seen by the GRS, N_{Al}, can be determined from knowledge of the spacecraft composition and geometry. However, in practice this quantity was difficult to determine with sufficient precision, as it reflects the solid-angle-weighted, post-attenuation amount of material within the spacecraft as observed by the GRS and was therefore left as an unknown quantity. Because of the similarity of the attenuation of 1014- and 2211-keV gamma-rays within a spacecraft-like composition [*Berger et al.*, 1987], N_{Al} is equivalent for both gamma rays. This leaves two equations (equations (9) and (10)) and three unknowns (N_{Al}, Φ_{1014}^p, and Φ_{2211}^p).

[18] The decision to leave N_{Al} as an unknown quantity necessitates the removal of either Φ_{1014}^p or Φ_{2211}^p as an unknown. This step was accomplished through the use of radiation transport codes for the production and transport of gamma rays within a planetary surface. These codes, coupled with forward modeling of gamma-ray transport and detector response, have been successfully applied to the analysis of GRS data from the Moon [e.g., *Prettyman et al.*, 2006] and Mars [*Boynton et al.*,

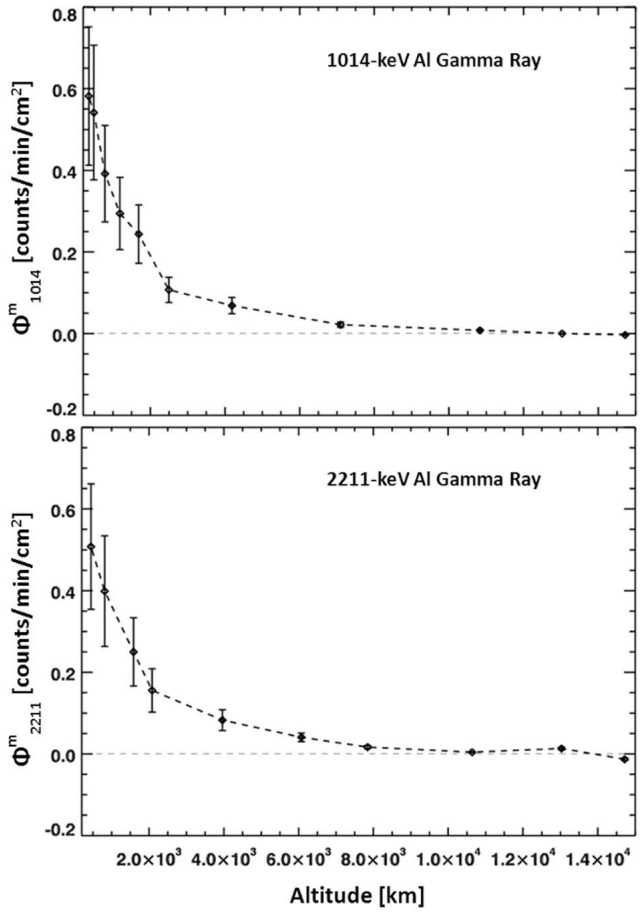

Figure 4. GRS-measured flux for the (top) 1014- and (bottom) 2211-keV Al gamma rays following the removal of the spacecraft-incident GCR background (equations (9) and (10)). Fluxes were calculated from the count rates in Figure 2 by dividing by the cross-sectional area of the detector (25.6 ± 4.5 cm^2; see Appendix B). The thin dashed line denotes a flux of zero, and the agreement between this value and the high-altitude fluxes demonstrates the removal of the high-altitude component of the measured gamma-ray flux.

2007]. The code developed for Mars Odyssey has been modified for the analysis of MESSENGER GRS data [*Evans et al.*, 2012] and was applied to this analysis to calculate the measured count-rate ratio for the two Al gamma rays. The modeled ratio between the 1014- and 2211-keV gamma-ray fluxes at the detector over all altitudes for an assumed surface composition [see *Evans et al.*, 2012] adopted on the basis of earlier MESSENGER geochemical measurements was found to be

$$\Phi^{p}_{2211} = (1.09 \pm 0.02)\Phi^{p}_{1014} \tag{11}$$

The error includes two sources; the first is the altitude dependence for this ratio, where that error was chosen to include all possible values of the ratio for the altitude range of the MESSENGER orbit, and the second is the uncertainty in the effective area of the detector, as the forward-model output was in the form of simulated count rates, which were therefore converted to fluxes using the same procedure as that utilized for the measured count rates (Appendix B). Casting Φ^{p}_{2211} as a function of Φ^{p}_{1014} leaves equations (9) and (10) with just two unknowns, N_{Al} and Φ^{p}_{1014}.

[19] Following the removal of the GCR-induced signal Φ^{GCR}_{γ} as detailed in equation (8), the measured 1014- and 2211-keV gamma ray fluxes were characterized as functions of the solid angle and are plotted in Figure 7. This procedure is based on the assumption of a linear relationship between the measured count rate and the solid angle. A linear fit of flux versus solid angle is supported by the data, but there may be a nonlinear dependence due to limb darkening [e.g., *Maurice et al.*, 2004] that would be consistent within the errors in these measurements (see Appendix A). Linear fits to these data and their errors resulted in empirically derived relations for the gamma-ray flux as a function of solid angle:

$$\Phi^{m'}_{1014} = A\Omega + B = (2.358 \pm 0.219)\Omega + (-0.014 \pm 0.002)\ \left[\text{min cm}^2\right]^{-1} \tag{12}$$

$$\Phi^{m'}_{2211} = C\Omega + D = (2.477 \pm 0.274)\Omega + (-0.014 \pm 0.004)\ \left[\text{min cm}^2\right]^{-1} \tag{13}$$

The near-zero values for B and D reflect the removal of Φ^{GCR}_{γ} from the data, as equation (8) requires $\Phi^{m\prime}_{\gamma}$ to be zero as $\Omega \rightarrow 0$. Their difference from zero suggests that the Φ^{GCR}_{γ} correction was slightly too large (~0.05%). As B and D are small, they are neglected, and equations (12) and (13) are compared with the empirically derived values A and C from equations (9)–(11) to yield

$$\left[2.358 \pm 0.219\ \frac{1}{\text{min cm}^2}\right]\Omega = \left[N_{Al}\int_{E\,\text{min}}^{\infty}\sigma_{1014}(E_n)N^{p}_{n}(E_n)\text{d}E + \Phi^{p}_{1014}\right]\Omega \tag{14}$$

$$\left[2.477 \pm 0.274\frac{1}{\text{min cm}^2}\right]\Omega = \left[N_{Al}\int_{Emin}^{\infty}\sigma_{2211}(E_n)N^{p}_{n}(E_n)\text{d}E + (1.09 \pm 0.02)\cdot\Phi^{p}_{1014}\right]\Omega \tag{15}$$

To solve for N_{Al} and Φ^{p}_{1014}, the solid angle dependence was divided out and the remaining components in these equations were calculated by evaluating the integrals in each equation from the modeled neutron fluxes (Figure 6) and experimentally measured gamma-ray production cross sections (Figure 5) to yield

$$\int_{E\text{min}}^{\infty}\sigma_{1014}(E_n)N^{p}_{n}(E_n)\text{d}E = 3.03 \times 10^{-25}\frac{\gamma}{\text{min}\,N_{Al}} \tag{16}$$

$$\int_{E\text{min}}^{\infty}\sigma_{2211}(E_n)N^{p}_{n}(E_n)\text{d}E = 2.18 \times 10^{-25}\frac{\gamma}{\text{min}\,N_{Al}} \tag{17}$$

Substituting these values into equation (15) and solving for N_{Al} gives

$$N_{Al} = (1.14 \pm 0.13) \times 10^{25} - [(5.01 \pm 0.09) \times 10^{24}]\Phi^{p}_{1014}\ \text{atoms} \tag{18}$$

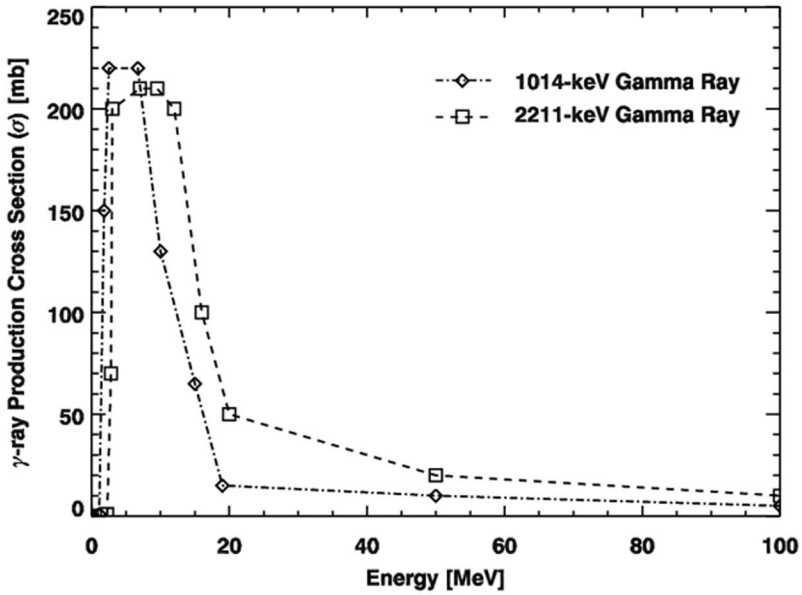

Figure 5. Gamma-ray production cross sections for the 1014- and 2211-keV neutron inelastic scattering reactions as a function of the incident neutron energy. These values originate from evaluated cross section data that were previously applied to the analysis of Mars Odyssey Gamma-Ray Spectrometer data [*Kim et al.*, 2007].

Substituting equation (18) into equation (14) results in a planetary-originating 1014-keV gamma-ray flux of 2.092 ± 0.856 g min^{-1} cm^{-2}. Dividing this number by the fitted 1014-keV gamma-ray flux (A, equation (15)) reveals that $89 \pm 37\%$ of the measured flux originates from the surface of Mercury. As is the convention throughout this manuscript, the quoted errors are the one-standard-deviation statistical errors of the measurements and the systematic errors previously mentioned (e.g., detector area, detection efficiency). As any value above 100% is unphysical, this value is recast as $88^{+12}_{-37}\%$.

[20] The final step in determining the Al abundance is to use the fitted peak values (Figure 1) to determine the portion of the measured 1014-keV count rate that is due to planetary gamma-ray emission. The average solid angle for the low-altitude data is 0.22, and following equation (8) we calculate

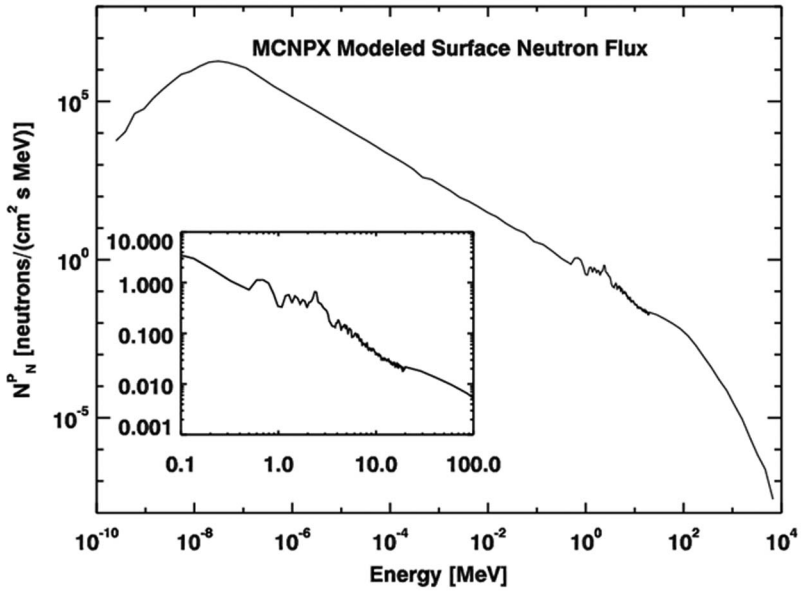

Figure 6. MCNPX-modeled neutron flux emanating from the surface of Mercury as a result of galactic-cosmic ray-induced nuclear spallation in the near surface (uppermost tens of centimeters). The structure observed in the energy range 1 to 10 MeV (inset) originates from resonant reactions within nuclei at these energies and also reflects higher-resolution simulations in this region.

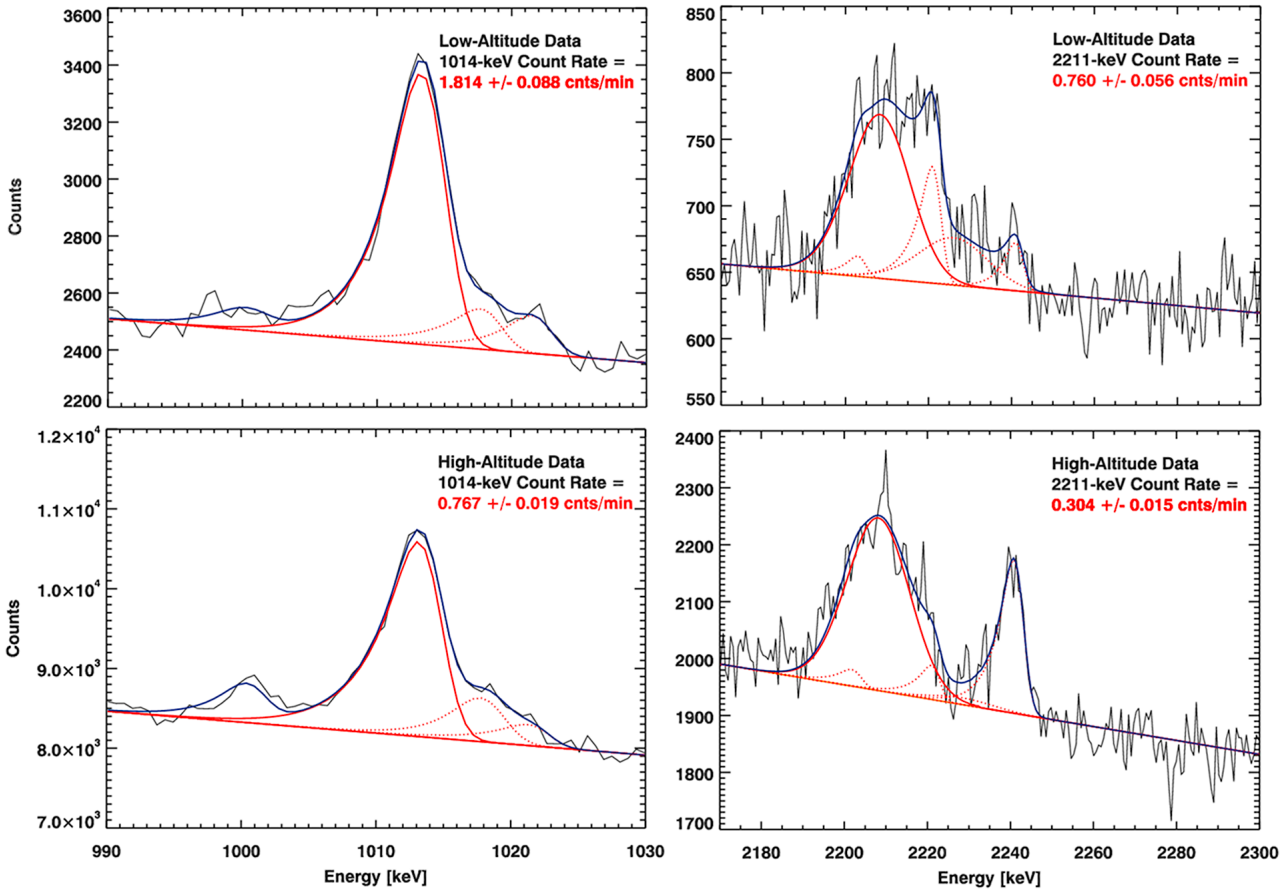

Figure 7. GRS-measured gamma-ray fluxes (Figure 3) as a function of the altitude-dependent solid angle (equation (2)). The dashed lines represent linear fits to the data following equations (12) and (13).

the low-altitude count rate without contributions from the GCR-induced signal ($C^{LA'}$) to be

$$C^{LA'}_{1014} = C^{LA}_{1014} - C^{HA}_{1014}[1 - \Omega_{LA}] = 1.22 \pm 0.16 \text{ counts min}^{-1} \quad (19)$$

where C^{LA} and C^{HA} are the low- and high-altitude count rates, respectively. The measured gamma-ray count rate originating from the surface of Mercury is then $C^{LA'} \times 88^{+12}_{-37}\% = 1.08^{+0.20}_{-0.47}$ counts min^{-1}. *Evans et al.* [2012] determined the 1779-keV Si planetary gamma-ray count rate to be 2.17 ± 0.03 counts/min, which provides a 1014/1779-keV count rate ratio of $0.50^{+0.09}_{-0.22}$. Comparing this value to the forward-model-derived count rate ratio of 0.39 for an assumed Al/Si abundance ratio of 0.23 provides a GRS-measured Al/Si abundance ratio of $0.29^{+0.05}_{-0.13}$.

5. Results and Implications

[21] The Al/Si ratio derived from the background reduction technique presented here ($0.29^{+0.05}_{-0.13}$) includes errors that originate from the statistical precision of the gamma-ray measurements and the fitting procedures carried out during this analysis, including the fits of the measured fluxes versus solid angle. In principle, additional errors are present that originate from uncertainties in our modeled Mercury neutron flux as well as from the nuclear reaction cross sections. However, a comparison of our values with those derived from the MESSENGER XRS [*Nittler et al.*, 2011] suggests that these errors may be minimal, since the XRS-derived Al/Si abundance ratios (0.17 ± 0.02 to 0.28 ± 0.03) are consistent with the one-standard-deviation uncertainties of the GRS-derived value. The two XRS footprints reported by *Nittler et al.* [2011] that overlap the GRS-measured regions produced values of 0.19 ± 0.03 and 0.22 ± 0.05, again consistent with the Al abundance derived from the 1014-keV gamma ray. Similarly, the XRS-derived, northern-hemisphere Al/Si abundance ratios presented by *Weider et al.* [2012] have an average value of 0.22 in the northern area of intercrater plains and heavily cratered terrain and 0.26 in the northern volcanic plains [*Head et al.*, 2011], which correspond to the two most common terrain types sampled by the GRS measurements. The nature of the MESSENGER orbit about Mercury, coupled with the selection of GRS data acquired at nadir angles of ≤45°, biased the present result to measurements taken over the northern volcanic plains (see Figure 2), and therefore the XRS value of 0.26 is most comparable to the GRS-derived value ($0.29^{+0.05}_{-0.13}$). Any comparison of GRS and XRS data should take note of the differences in the sampling depths of the techniques, as X-ray spectroscopy is sensitive to elemental composition within ≤100 μm of the surface compared with the sensitivity of gamma-ray spectroscopy to the uppermost tens of centimeters.

[22] Like the XRS results, the GRS-derived Al/Si abundance ratio differs significantly from those of lunar highlands material (0.6–0.9) [*Papike et al.*, 1998] but is consistent with those of terrestrial komatiites (0.1–0.3) and basalts (0.2–0.4) [*Lodders and Fegley*, 1998]. This finding supports the conclusion of *Nittler et al.* [2011] that a global, plagioclase-rich crust similar to that of the lunar highlands may be ruled out. The GRS-measured Al/Si abundance ratio is also consistent with compositions resulting from partial melts of CB (0.35) [*Taylor and Scott*, 2003] or enstatite (0.3) [*McCoy et al.*, 1999] chondrites, supporting the conclusions of *Peplowski et al.* [2011b] and *Nittler et al.* [2011] that the near-surface composition of Mercury is consistent with that of a planet that formed from highly reduced precursor material, perhaps akin to enstatite chondrite meteorites.

[23] These results also have implications for previously reported MESSENGER GRS measurements. *Rhodes et al.* [2011] reported an analysis of GRS data acquired during the three MESSENGER flybys of Mercury prior to orbit insertion. Their analysis used the 1014-keV Al gamma-ray to define a "background amplification factor" (A_{BG}) as

$$A_{BG} = \frac{C^{\mathrm{Low}}}{C^{\mathrm{High}}} \tag{20}$$

where C^{Low} and C^{High} are the measured count rates in the low- and high-altitude spectra, respectively. In terms of the source component analysis technique presented here, equation (20) corresponds to

$$A_{BG} = \frac{\left[C^{\mathrm{P}} + C^{\mathrm{N}} + C^{\mathrm{GCR}}\right]^{\mathrm{Low}}}{\left[C^{\mathrm{GCR}}\right]^{\mathrm{High}}} \tag{21}$$

where C^{P}, C^{N}, and C^{GCR} are the altitude-dependent count rates originating from planetary gamma-ray emission, planetary neutron-induced emission within the spacecraft, and GCR-induced emission within the spacecraft, respectively. The altitude dependencies of these components are described in equation (1). Since the GRS is surrounded by Al, and in the absence of any supporting measurements from the XRS during the flybys, *Rhodes et al.* [2011] assumed that for the 1014-keV line, $C^{\mathrm{N}} \gg C^{\mathrm{P}}$, such that equation (21) was reduced to:

$$A_{BG} \rightarrow \frac{\left[C^{\mathrm{GCR}} + C^{\mathrm{N}}\right]^{\mathrm{low}}}{\left[C^{\mathrm{GCR}}\right]^{\mathrm{high}}} \tag{22}$$

In this scenario, the measured A_{BG} (equation (20)) describes the low-altitude background $C^{\mathrm{N}} + C^{\mathrm{GCR}}$ in terms of its magnitude relative to the high-altitude background C^{GCR}. Analysis of the 1014-keV Al peak measurements from the flybys provided a background amplification factor of 2.10 ± 0.4. This factor was used to determine the backgrounds for the Fe, Ti, and Si gamma rays presented in that work by multiplying the high-altitude count rates by A_{BG} to determine the low-altitude backgrounds. With these background estimates, *Rhodes et al.* [2011] provided the first measurements of the elemental composition of the surface of Mercury from MESSENGER.

[24] The source component analysis procedure presented here indicates that the planetary-originating contribution to the measured 1014-keV gamma ray is 88^{+12}_{-37}%, meaning that the assumption of $C^{\mathrm{N}} \gg C^{\mathrm{P}}$ was not valid. On the basis of MESSENGER XRS measurements that indicate low Ti abundances (<1 wt%) on the surface of Mercury [*Nittler et al.*, 2011], the 983-keV Ti peak meets the requirement of $C^{\mathrm{N}} \gg C^{\mathrm{P}}$ and was therefore used to determine the background amplification factor (1.49 ± 0.10) derived by *Peplowski et al.* [2012] and utilized by *Evans et al.* [2012] to determine the abundances of stable elements on the surface of Mercury. Amplification factors are altitude dependent, and the Ti-derived amplification factor was determined using an elevation cutoff for the low-altitude data of 2000 km, which differs from the cutoff of 2500 km utilized by *Rhodes et al.* [2011] to derive their amplification factor of ~2. The difference in the two altitude cutoffs suggests that the divergence between the two amplification factors is larger than suggested by a simple comparison of the two values. As a result, the background corrections of *Rhodes et al.* [2011] overestimate the low-altitude backgrounds and therefore underestimate the planetary signal for the flyby measurements. Later publications on the analysis of orbital data [*Peplowski et al.*, 2011b, 2012; *Evans et al.*, 2012] should be referenced for accurate abundances.

[25] Application of the Ti-derived background amplification factor to elements other than Ti requires scaling by the relative integrated cross sections, as each element has a different cross section and samples a distinct portion of the energy-dependent neutron flux. For example, taking the ratio of the integrated cross section for the 983-keV Ti line to that for the 6129-keV O line yields

$$\frac{\int_{983\ \mathrm{keV}}^{\infty} \sigma_{983}(E_n) N_{\mathrm{n}}^{\mathrm{p}}(E)\mathrm{d}E}{\int_{6129\ \mathrm{keV}}^{\infty} \sigma_{6129}(E_n) N_{\mathrm{n}}^{\mathrm{p}}(E)\mathrm{d}E} = 2.86 \tag{23}$$

where σ_{983} is the 983-keV gamma-ray production cross section for neutron inelastic scattering on Ti, and σ_{6129} is the 6129-keV gamma-ray production cross section for neutron inelastic scattering on O. The difference between the integrated cross sections is primarily attributable to the energy-dependence of the planetary neutron flux (see Figure 6), as the 6129-keV threshold limits the gamma-ray production to excitation by the portion of the planetary neutron flux with an integrated number of neutrons much smaller than the equivalent integral with a threshold of 983 keV. As a result, we expect that the 6129-keV spacecraft backgrounds originating from excitation by planet-originating neutrons will have a flux that is a factor of 2.86 less than that of the 983-keV peak. This result means that Ti is a better choice for defining a background amplification factor than Al, but that any amplification factor derived from a single peak must be modified by the ratio of the cross sections (e.g., equation (23)) before being applied to other gamma-ray peaks as was done by *Evans et al.* [2012].

6. Further Applications

[26] The background reduction technique presented here has been successfully applied to the measurement of Al on the surface of Mercury. This technique can also be applied to

other elements, as well as data from other gamma-ray spectrometers, provided the altitude-dependent gamma-ray flux for two gamma rays from a given element can be measured and characterized with forward modeling. Examples of other elements for which this procedure may be carried out in the MESSENGER GRS data set include Ti (983- and 1312-keV) and Fe (846- and 1238-keV), although the analysis of these peaks is complicated by the frequent activation of long-lived radioisotopes with identical gamma decays by solar energetic proton events, and by the low planet-originating fluxes for these gamma rays. In principle, it is also possible to use this method to analyze gamma rays originating from neutron capture reactions. However, this procedure is complicated by the moderation of the planetary neutron flux to thermal energies within the spacecraft as well as the altitude dependence of thermal neutrons, which are gravitationally bound to the planet and therefore have a different altitude dependence from that for fast neutrons.

[27] Gamma-ray measurements made with any spacecraft that varies markedly in altitude can benefit from this procedure. For example, it may be possible to use this procedure for the analysis of data from the Gamma-Ray and Neutron Detector (GRaND) instrument on the Dawn spacecraft [*Prettyman et al.*, 2011]. This instrument, like the MESSENGER GRS, is body mounted and therefore measures spacecraft-originating backgrounds in addition to the planetary signal of interest. GRaND operated during the slow approach of Dawn to Vesta, the high-altitude (680 km) orbital mapping, and the transfer to and operation in the low-altitude (210 km) mapping orbit. As a result, the altitude dependence of the GRaND-measured gamma-ray peaks can be characterized, facilitating the use of the source component analysis technique presented here.

Appendix A: Non-isotropic Solid Angle

[28] For this work we assume an isotropic solid-angle dependence for neutron and gamma-ray emission from the surface of Mercury. Fits to the measured 1014- and 2211-keV fluxes versus solid angle (Figure 7) support this assumption, although some anisotropy is consistent within the errors of the data. The magnitude of the Al flux errors, coupled with the fact that the measurements include contributions from both Φ_γ^n and Φ_γ^p, prohibits using the Al measurements to determine the magnitude of any non-isotropic neutron and gamma-ray emission. Other MESSENGER measurements are combined with previous analysis of Lunar Prospector (LP) data to better constrain non-isotropic emission in the MESSENGER Al gamma-ray measurements and its impact on the assumed solid-angle dependence used in this analysis.

[29] Non-isotropic neutron emission has been observed in LP Neutron Spectrometer (LPNS) measurements of the lunar neutron albedo by *Maurice et al.* [2004], who defined the solid angle as

$$\Omega(\mathrm{h}) = [1 - \cos\theta_{\max}(h)] \tag{A1}$$

where h is the same as for equation (2) and $\theta_{\max}$ is θ_L. Here $\Omega(h)$ is the fraction of 2π sr subtended by the field of view of the planet, which differs from the definition in equation (2), i.e., the fraction of 4π sr. MCNPX models of planetary neutron emission were used to develop a function to describe

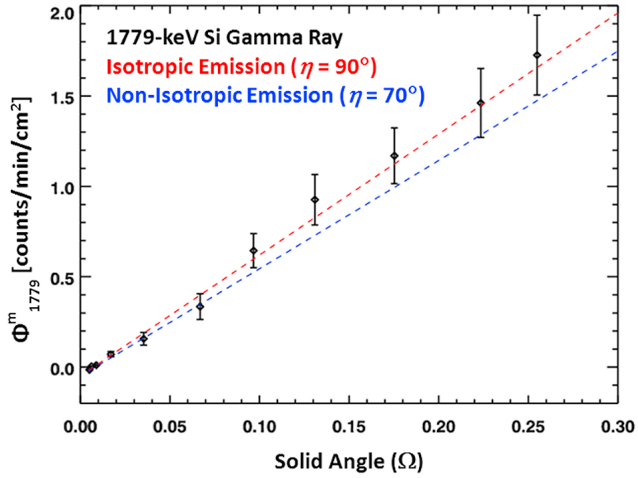

Figure A1. The 1779-keV Si gamma-ray flux as a function of solid angle (Ω). Lines indicating (red) isotropic gamma-ray emission (equation (A2), $\eta = 90°$) and (blue) the maximum non-isotropic emission allowed by the data ($\eta = 70°$) to within the one-standard-deviation errors are included.

non-isotropic solid-angle emission due to limb darkening by modifying equation (A1) as

$$\Omega(\mathrm{h}) = (1 - \cos\nu(\mathrm{h})) \tag{A2}$$

where

$$\nu(\mathrm{h}) = \left(\frac{R_m}{R_m + \mathrm{h}}\sin\eta\right) \tag{A3}$$

Here, η is a parameter that describes the degree of the non-isotropic neutron emission, with an η value of 90° representing isotropy. LPNS measurements of lunar neutrons over an altitude range of 10 to 4000 km were used to empirically derive an η value of 80°.

[30] The formalism of *Maurice et al.* [2004] has been applied to MESSENGER Neutron Spectrometer (NS) measurements of fast (>700 keV) neutrons from Mercury as part of the ongoing analysis of MESSENGER NS data. Removing the effects of the spatially dependent detection efficiency of the MESSENGER NS, an η value of 75° was determined, close to the lunar value of 80°. In the altitude range of the MESSENGER orbit about Mercury (200 to 15,200 km), the deviation between the isotropic and non-isotropic emission increases with increasing solid angle. For $\eta = 75°$, the difference is ≤10%, with the isotropic case overestimating the neutron flux from non-isotopic emission. Including this factor in the analysis presented in section 4 would correspond to a smaller contribution from Φ_γ^n to Φ_γ^m, as fewer neutrons are reaching the spacecraft than has been assumed. As the final result is already inclusive of $\Phi_\gamma^n = 0$ within the one-standard-deviation errors, including non-isotropic neutron emission does not modify the results presented here.

[31] The 1779-keV Si gamma ray has a higher count rate than the Al gamma rays and is known to have minimal contributions from GCR- and planetary-neutron-induced gamma-ray production [*Evans et al.*, 2012]. As a result, it serves as the best empirical measure of non-isotropic gamma-ray emission. Following the peak analysis procedure outlined by *Peplowski et al.* [2012], the 1779-keV count rate has been determined as a function of solid angle using data acquired at an angle θ_n from

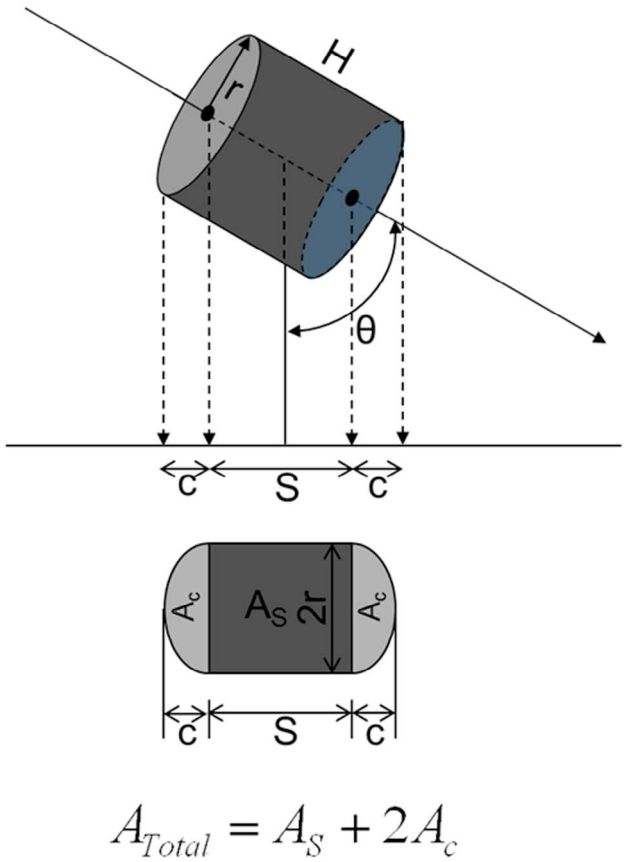

Figure B1. The coordinate system used to derive the cross-sectional area of the high-purity Ge crystal of the MESSENGER Gamma-Ray Spectrometer [*Goldsten et al.*, 2007] as seen from the surface of Mercury.

the nadir direction of 15° or less. This stringent nadir-angle restriction ensures that any measured variation is not the result of variable viewing geometry. The 1779-keV count rates are converted to gamma-ray fluxes (see section 3 and Appendix B) and plotted versus solid angle in Figure A1. As was the case with the 1014- and 2211-keV lines, a linear relation between the measured flux and solid angle is found to be consistent with the data, although some non-isotropy ($\eta \geq 70°$) is permitted within the one-standard-deviation errors. This result is consistent with the measured η for fast neutrons measured with the MESSENGER NS and demonstrates that there is no measurable difference between the solid-angle dependencies for neutrons and gamma rays reaching the spacecraft.

Appendix B: Detector Cross-Sectional Area

[32] Deriving measured gamma-ray fluxes from measured count rates requires dividing by the cross-sectional area of the detector as seen by the planet. Unlike previous gamma-ray spectroscopy experiments, which maintained planet-facing orientations throughout their orbital observations, the MESSENGER GRS frequently points off-nadir [*Peplowski et al.*, 2012]. As a result, the area of the detector varies throughout the data set used in this analysis. The gamma-ray-sensitive volume of the GRS is a cylindrical crystal of high-purity Ge [*Goldsten et al.*, 2007], and the total area of a cylinder (A_T) projected onto a surface as a function of angle is

$$A_T = A_s + 2A_c = 2rH\sin\theta + \pi r^2\cos\theta \quad \text{(B1)}$$

where r and H are the radius and height of the cylinder, respectively, and θ is the angle between the cylinder axis and the nadir direction. A_c and A_s, along with the coordinate system for this system, are shown in Figure B1. The dimensions of the cylinder are 5 cm diameter by 5 cm length, and the nadir angle θ_n is equivalent to θ, making equation (B1) equivalent to

$$A_T(\theta_n) = 25\ \text{cm}^2\sin\theta_n + 19.6\ \text{cm}^2\cos\theta_n \quad \text{(B2)}$$

which has a minimum area of 19.6 cm^2 at 0° and a maximum area of 31.8 cm^2 at 38°.

[33] The distribution of nadir angles found in this data set is shown in Figure B2, which includes a maximum allowed value of 45° in the low-altitude (<2000 km) range to limit the attenuation of gamma rays by GRS-surrounding

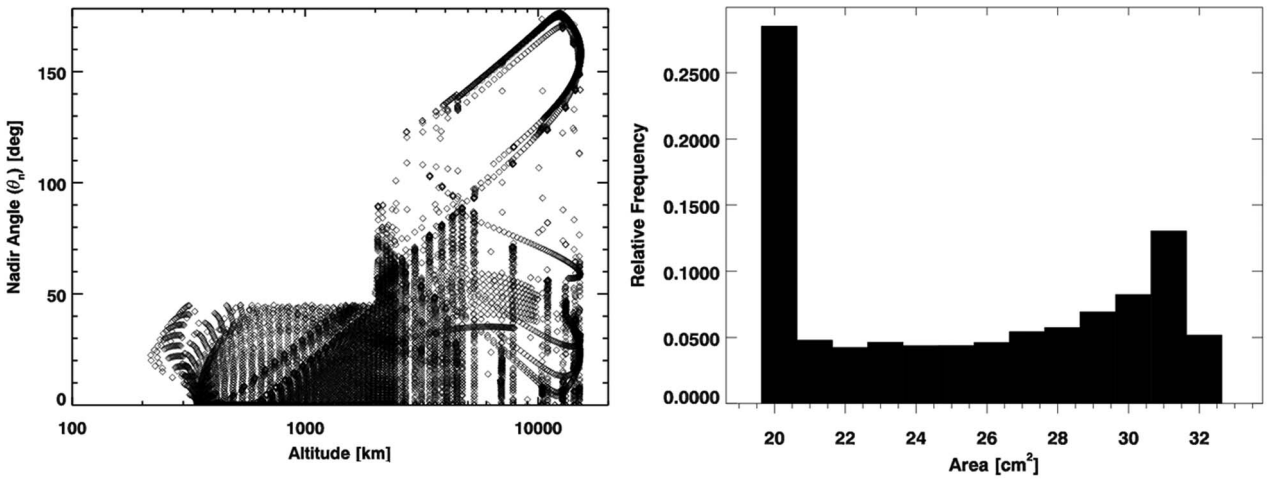

Figure B2. (left) Allowed values for the nadir angle of the MESSENGER GRS as a function of altitude for each individual spectrum used in this analysis. (right) A histogram of the corresponding values for the cross-sectional area shows the range and distribution of the areas utilized in this analysis.

Table C1. Mercury Surface Composition Adopted for MCNPX Calculations of Neutron Flux

Element	Isotope[a]	Abundance (wt%)
Oxygen	^{16}O	44.89
Magnesium	^{24}Mg	12.2
Aluminum	^{27}Al	5.73
Silicon	^{28}Si	24.4
Sulfur	^{32}S	2.20
Chlorine	^{35}Cl, ^{37}Cl	0.15, 0.05
Potassium	^{39}K	0.10
Calcium	^{40}Ca	4.88
Titanium	^{44}Ti	0.78
Chromium	^{50}Cr, ^{52}Cr, ^{53}Cr, ^{54}Cr	0.02, 0.41, 0.05, 0.01
Manganese	^{55}Mn	0.49
Iron	^{54}Fe, ^{56}Fe, ^{57}Fe, ^{58}Fe	0.21, 3.36, 0.08, 0.01

[a]Individual isotopes are included for elements whose neutron-absorbing cross sections vary appreciably for each isotope. The surface composition was taken from initial MESSENGER geochemical results [*Lawrence et al.*, 2010; *Nittler et al.*, 2011; *Peplowski et al.*, 2011b].

spacecraft components [*Peplowski et al.*, 2012]. These allowed nadir angles permit a large number of possible values for $A_T(\theta_n)$, which are also shown in Figure B2. For each altitude range considered in this analysis (Figure 3), the mean and standard deviation of the detector area were calculated (25.6 ± 4.5 cm^2) and used to convert the measured count rates to the gamma-ray flux at the detector (Figure 4).

Appendix C: Planetary Neutron Flux

[34] The surface neutron flux used in this analysis was calculated following the methodology of *Lawrence et al.* [2010], which was based on previous calculations for lunar soils [*McKinney et al.*, 2006; *Lawrence et al.*, 2006]. These calculations used the Monte Carlo particle transport code MCNPX [*Pelowitz*, 2005] to create full-planet simulations of GCR-induced neutron emission from the surface of Mercury. The input for these models is an assumed surface composition (see Table C1) and an incident GCR proton flux. The GCR energy-dependent flux spectrum was characterized using the parameterization for protons and alpha particles given by *Masarik and Reedy* [1996] that depends on a solar modulation parameter, ϕ, to characterize both the shape and absolute normalization of the spectrum. To obtain the solar modulation parameter, Earth-based south-pole neutron monitor data from the Bartol Research Institute Neutron Monitor (University of Delaware Bartol Research Institute Neutron Monitor Program, http://neutronm.bartol.udel.edu) were used in conjunction with the procedure of *McKinney et al.* [2006] to estimate that ϕ = 461 MV during the data acquisition period considered here. This value corresponds to an incident particle normalization of 4.44 particles cm^{-2} s^{-1}, which was used to normalize the output of the MCNPX models to produce the absolute neutron flux (Figure 6). The use of absolute neutron fluxes is justified by previous work that has benchmarked similar simulations to Apollo 17 drill-core neutron measurements [*McKinney et al.*, 2006] as well as MESSENGER NS flyby measurements of planetary neutron emission [*Lawrence et al.*, 2010], the latter of which demonstrated an ability to model the absolute neutron count rates to better than 10%. On that basis, the absolute neutron flux simulated here was used to determine the spacecraft-originating gamma-ray fluxes for the 1014- and 2211-keV Al gamma rays (see section 4).

[35] **Acknowledgments.** We thank the entire MESSENGER team for their efforts developing, building, launching, navigating, and operating the spacecraft. We also thank S. Z. Weider, as well as two anonymous reviewers, for reviewing the manuscript and providing helpful comments. MESSENGER is administered under NASA's Discovery Program under contract NAS5–97271 to The Johns Hopkins University Applied Physics Laboratory and NASW-00002 to the Carnegie Institution of Washington.

References

Berger, M. J., J. H. Hubbell, S. M. Seltzer, J. Chang, J. S. Coursey, R. Sukumar, D. S. Zucker, and K. Olsen (1987), XCOM: Photon cross sections on a personal computer, *Rep. NBSIR 87–3597*, Natl. Inst. of Stand. and Technol., Gaithersburg, Md.

Bielefeld, M. J., R. C. Reedy, A. E. Metzger, J. I. Trombka, and J. R. Arnold (1976), Surface chemistry of selected lunar regions, *Proc. Lunar Sci. Conf.*, *7th*, 2661–2676.

Boynton, W. V., et al. (2004), The Mars Odyssey Gamma-Ray Spectrometer instrument suite, *Space. Sci. Rev.*, *110*, 37–83, doi:10.1023/B:SPAC.0000021007.76126.15.

Boynton, W. V., et al. (2007), Concentration of H, Si, Cl, K, Fe, and Th in the low- and mid-latitude regions of Mars, *J. Geophys. Res.*, *112*, E12S99, doi:10.1029/2007JE002887.

Evans, L. G., R. C. Reedy, R. D. Starr, K. E. Kerry, and W. V. Boynton (2006), Analysis of gamma ray spectra measured by Mars Odyssey, *J. Geophys. Res.*, *111*, E03S04, doi:10.1029/2005JE002657.

Evans, L. G., et al. (2012), Major element abundances on the surface of Mercury: Results from the MESSENGER Gamma-Ray Spectrometer, *J. Geophys. Res.*, *117*, E00L07, doi:10.1029/2012JE004178.

Feldman, W. C., et al. (2004), Gamma-Ray, Neutron, and Alpha-Particle Spectrometers for the Lunar Prospector mission, *J. Geophys. Res.*, *109*, E07S06, doi:10.1029/2003JE002207.

Feldman, W. C., et al. (2010), Evidence for extended acceleration of solar flare ions from 1–8 MeV solar neutrons detected with the MESSENGER Neutron Spectrometer, *J. Geophys. Res.*, *115*, A01102, doi:10.1029/2009JA014535.

Goldsten, J. O., et al. (1997), The X-Ray/Gamma-Ray Spectrometer on the Near Earth Asteroid Rendezvous mission, *Space Sci. Rev.*, *83*, 169–216, doi:10.1023/A:100505272076.

Goldsten, J. O., et al. (2007), The MESSENGER Gamma-Ray and Neutron Spectrometer, *Space Sci. Rev.*, *131*, 339–391, doi:10.1007/s11214-007-9262-7.

Hasebe, N., et al. (2008), The high precision gamma-ray spectrometer for lunar polar orbiter SELENE, *Adv. Space Res.*, *42*, 323–330, doi:10.1016/j.asr.2007.05.046.

Head, J. W., et al. (2011), Flood volcanism in the northern high latitudes of Mercury revealed by MESSENGER, *Science*, *333*, 1853–1856, doi:10.1126/science.1211997.

Kim, K. J., D. M. Drake, R. C. Reedy, R. M. S. Williams, and W. V. Boynton (2007), Theoretical fluxes of gamma rays from the Martian surface, *J. Geophys. Res.*, *112*, E03S09, doi:10.1029/2005JE002655.

Lawrence, D. J., W. C. Feldman, B. L. Barraclough, A. B. Binder, R. C. Elphic, S. Maurice, and D. R. Thomsen (1998), Global elemental maps of the Moon: The Lunar Prospector Gamma-Ray Spectrometer, *Science*, *281*, 1484–1489, doi:10.1126/science.281.5382.1484.

Lawrence, D. J., W. C. Feldman, R. C. Elphic, J. J. Haggerty, S. Maurice, G. W. McKinney, and T. H. Prettyman (2006), Improved modeling of Lunar Prospector Neutron Spectrometer data: Implications for hydrogen deposits at the lunar poles, *J. Geophys. Res.*, *111*, E08001, doi:10.1029/2005JE002637.

Lawrence, D. J., W. C. Feldman, J. O. Goldsten, T. J. McCoy, D. T. Blewett, W. V. Boynton, L. G. Evans, L. R. Nittler, E. A. Rhodes, and S. C. Solomon (2010), Identification and measurement of neutron-absorbing elements on Mercury's surface, *Icarus*, *209*, 195–209, doi:10.1016/j.icarus.2010.04.005.

Lodders, K., and B. Fegley Jr. (1998), *The Planetary Scientist's Companion*, 371 pp., Oxford Univ. Press, New York.

Masarik, J., and R. C. Reedy (1996), Gamma ray production and transport in Mars, *J. Geophys. Res.*, *101*, 18,891–18,912, doi:10.1029/96JE01563.

Maurice, S., D. J. Lawrence, W. C. Feldman, R. C. Elphic, and O. Gasnault (2004), Reduction of neutron data from Lunar Prospector, *J. Geophys. Res.*, *109*, E07S04, doi:10.1029/2003JE002208.

McCoy, T. J., T. L. Dickenson, and G. E. Lofgren (1999), Partial melting of the Indarch (EH4) meteorite: A textural, chemical, and phase relations

view of melting and melt migration, *Meteorit. Planet. Sci.*, *34*, 735–746, doi:19.111/j.1945–5100.1999.tb01386.x.

McKinney, G. W., D. J. Lawrence, T. H. Prettyman, R. C. Elphic, W. C. Feldman, and J. J. Hagerty (2006), MCNPX benchmark for cosmic ray interactions with the Moon, *J. Geophys. Res.*, *111*, E06004, doi:10.1029/2005JE002551.

Nittler, L. R., et al. (2011), The major element composition of Mercury's surface from MESSENGER X-ray spectrometry, *Science*, *333*, 1847–1850, doi:10.1126/science.1211567.

Papike, J. J., G. Ryder, and C. K. Shearer (1998), Lunar samples, in *Planetary Materials, Rev. Miner.*, vol. 36, edited by J. J. Papike, pp. 5-001–5-234, Miner. Soc. of Am., Washington, D. C.

Pelowitz, D. B. (Ed.) (2005), MCNPX user's manual, version 2.5.0, *Rep. LA-UR-94–1817*, 473 pp., Los Alamos Natl. Lab., Los Alamos, N. M.

Peplowski, P. N., D. T. Blewett, B. W. Denevi, L. G. Evans, D. J. Lawrence, L. R. Nittler, E. A. Rhodes, C. M. Selby, and S. C. Solomon (2011a), Mapping iron abundances on the surface of Mercury: Predicted spatial resolution of the MESSENGER Gamma-Ray Spectrometer, *Planet. Space Sci.*, *59*, 1654–1658, doi:10.1016/j.pss.2011.06.001.

Peplowski, P. N., et al. (2011b), Radioactive elements on Mercury's surface from MESSENGER: Implications for the planet's formation and evolution, *Science*, *333*, 1850–1852, doi:10.1126/science.1211576.

Peplowski, P. N., et al. (2012), Variations in the abundances of potassium and thorium on the surface of Mercury: Results from the MESSENGER Gamma-Ray Spectrometer, *J. Geophys. Res.*, *117*, E00L04, doi:10.1029/2012JE004141.

Prettyman, T. H., J. J. Hagerty, R. C. Elphic, W. C. Feldman, D. J. Lawrence, G. W. McKinney, and D. T. Vaniman (2006), Elemental composition of the lunar surface: Analysis of gamma ray spectroscopy data from Lunar Prospector, *J. Geophys. Res.*, *111*, E12007. doi:10.1029/2005JE002656.

Prettyman, T. H., et al. (2011), Dawn's Gamma Ray and Neutron Detector, *Space Sci. Rev.*, *163*, 371–459, doi:10.1007/s11214-011-9862-0.

Reedy, R. C. (1978), Planetary gamma-ray spectroscopy, *Proc. Lunar Planet. Sci. Conf.*, *9th*, 2961–2984.

Rhodes, E. A., et al. (2011), Analysis of MESSENGER Gamma-Ray Spectrometer data from the Mercury flybys, *Planet. Space Sci.*, *59*, 1829–1841, doi:10.1016/j.pss.2011.07.018.

Solomon, S. C., R. L. McNutt Jr., R. E. Gold, and D. L. Domingue (2007), MESSENGER mission overview, *Space Sci. Rev.*, *131*, 3–39, doi:10.1007/s11214-007-9247-6.

Taylor, G. J., and E. R. D. Scott (2003), Mercury, in *Meteorites, Comets, and Planets, Treatise on Geochemisty*, vol. 1, edited by A. M. Davis, pp. 477–485, Elsevier-Pergamon, Oxford, U. K.

Trombka, J. I., et al. (2001), The NEAR-Shoemaker X-ray/gamma-ray spectrometer experiment: Overview and lessons learned, *Meteorit. Planet. Sci.*, *36*, 1605–1616, doi:10.1111/j.1945-5100.2001.tb01852.x.

Weider, S. Z., L. R. Nittler, R. D. Starr, T. J. McCoy, K. R. Stockstill-Cahill, P. K. Byrne, B. W. Denevi, J. W. Head, and S. C. Solomon (2012), Chemical heterogeneity on Mercury's surface revealed by the MESSENGER X-Ray Spectrometer, *J. Geophys. Res.*, *117*, E00L05, doi:10.1029/2012JE004153.

Yamashita, N., et al. (2010), Uranium on the Moon: Global distribution and U/Th ratio, *Geophys. Res. Lett.*, *37*, L10201, doi:10.1029/2010GL043061.